JOURNAL OF CATALYSIS 113, 25–35 (1988)

Oxidative Coupling of Methane over Na^+- and Rb^+-Doped MgO Catalysts

E. IWAMATSU, T. MORIYAMA, N. TAKASAKI, AND K. AIKA[1]

Research Laboratory of Resources Utilization, Tokyo Institute of Technology, 4259 Nagatsuta, Midori-ku, Yokohama 227, Japan

Received August 18, 1987; revised March 22, 1988

The promoter effect of Na^+ and Rb^+ on MgO catalysts was studied for the oxidative coupling of methane. The maximum yield and selectivity obtained for the formation of C_2 hydrocarbons (C_2H_6 + C_2H_4) from CH_4 and O_2 were 22.4% (1073 K) and 57% (1023 K), respectively, over 2 g of 15 mol% Na^+–MgO catalyst. Physical factors of the promoted MgO catalysts were investigated with BET, SEM, and XRD techniques and were compared with the activities. Alkali metal ions, the promoters, caused structural changes in MgO. Those changes, which are related to the activity of C_2 hydrocarbon formation, are classified in two categories: (1) surface activation through the lattice distortion, and (2) specific surface area reduction. When catalysts with the same specific surface areas were compared, alkali ion-doped MgO in which extensive line broadening is observed by XRD was more active than pure MgO. On the other hand, a sintered pure MgO with low specific surface area showed higher C_2 hydrocarbon yield than unsintered pure MgO. The two factors are discussed in relation to the reaction mechanism.

INTRODUCTION

Recently, utilization of natural gas, especially the conversion of methane to such chemicals as ethylene and methanol, has been studied widely. In particular, the oxidative coupling of methane (*1–18*) has been studied over various catalysts. Many works stress a promoter effect for the alkali, for example, Na^+–PbO–Al_2O_3 (*2*), Li^+–MgO (*3a–c*), Li^+–Sm_2O_3 (*4b*), Li^+–ZnO (*7*), Na^+–MgO (*5a*). Hinsen *et al.* have reported that the addition of alkali neutralizes the acidic site which is effective for the complete oxidation (*2b*). Ito and Lunsford have reported that [Li^+O^-] centers produced by Li^+ doping of MgO are effective for the oxidative coupling (*3a–c*). The authors have pointed out the importance of the morphology, i.e., a specific surface area (*5c*). Many works seem to stress a sole factor for the catalyst activities, and do not discuss multiple factors including a morphological factor.

Since, among the catalysts studied, alkali-doped MgO catalysts are active and selective for C_2 hydrocarbon formation, especially at 973 to 1023 K, it is worthwhile studying them in detail. In this work, Na^+–MgO and Rb^+–MgO catalysts, the most effective of the promoted MgO catalysts (*5a*), have been investigated to clarify the alkali promoter effect. As a consequence, it was found that addition of alkali causes extensive line broadening in XRD and a specific surface area reduction, both of which are discussed in relation to the reaction mechanism of C_2 hydrocarbon formation.

EXPERIMENTAL

The reaction was performed in a conventional flow reactor (8-mm o.d.) at temperatures between 673 and 1073 K. CH_4, air, and He were charged with flow rates of 1.5 ml min^{-1} (4.02 mmol h^{-1}), 3.75 ml min^{-1}, and 50 ml min^{-1}, respectively. The ratio of CH_4/O_2 was 2.0 ± 0.1 ($2CH_4 + O_2 = C_2H_4 + 2H_2O$). Selectivity and yield are defined as (2 × moles C_2 hydrocarbons produced)/(moles CH_4 reacted) and (2 × moles C_2 hy-

[1] To whom correspondence should be addressed.

0021-9517/88 $3.00

drocarbons produced)/(moles CH_4 in the feed), respectively. Metal nitrates were added to MgO (Soekawa Chemical Co., 99.75%) in water; then the samples were dried, pelletted, and weighed. The mol% of the promoter is the molar ratio of the promoter against MgO. A pure MgO sample was prepared by soaking in water and pelletting. Two grams of sample was evacuated or treated in He flow at 773 K for 1 h and then at 1073 K for 2 h and used for the reaction. The reactants and products were analyzed on a gas chromatograph (FID, TCD) with Porapak Q and MS 5A columns. Specific surface area of the heated sample was measured by BET method using N_2 adsorption at 77 K. SEM pictures of the same samples were taken with a Hitachi HFS-2 or SEM-800 in Naka Works, Hitachi Ltd. Application Laboratory. XRD spectra were taken with a Rigaku 2027. ESR spectra were taken with a JEOL JES-FE-1X spectrometer. Alkali metals on MgO may evaporate at high temperatures. Content of Na^+ and Rb^+ was measured before and after a heat treatment–reaction cycle by atomic adsorption (AA) for Na^+ and inductively coupled plasma spectrometry (ICP) for Rb^+.

RESULTS

Relationship between Specific Surface Area and C_2 Yield

General characteristics of the title reaction over promoted MgO catalysts have already been reported (*5d*). The main products are C_2H_6, C_2H_4, CO_2, H_2O, and some CO. Amounts of other products such as propane are negligible (*19*). Both CO_2 and C_2 hydrocarbons (C_2H_6, C_2H_4) appear at the same temperature when the reaction temperature is raised over Na^+–MgO and Rb^+–MgO. A carbon balance of 100 ± 10% was obtained for every run over the two series of catalysts in half an hour. C_2 hydrocarbons were obtained in the reaction at 1023 K over Na^+–MgO and their specific surface areas are plotted as a function of Na^+ expected content (Na^+ content in the starting sample) in Fig. 1. As will be shown later, the actual content is lower than the expected content, the expression usually used because of its importance in this work. With increasing Na^+ expected content, the specific surface area generally decreases and C_2 hydrocarbon yield increases. It should also be pointed out that 0.2 mol% Na^+–MgO has extraordinarily high specific surface area (212 $m^2\ g^{-1}$). When 10, 15, and 20 mol% Na^+ is added, the specific surface areas are as low as 1–2 $m^2\ g^{-1}$, and a maximum C_2 hydrocarbon yield of ca. 20% is obtained over 15% Na^+–MgO. Similar results are obtained for Rb^+–MgO catalysts, as is shown in Fig. 2. In this case, with Rb^+ content increasing to 5 mol%, the specific surface area decreases to 24 $m^2\ g^{-1}$ and C_2 hydrocarbon yield increases to ca. 15%. Above 5 mol%, the specific surface area increases and C_2 hydrocarbon yield decreases. From these results, specific surface area seems to be one of the important factors in the effective production of C_2 hydrocarbons.

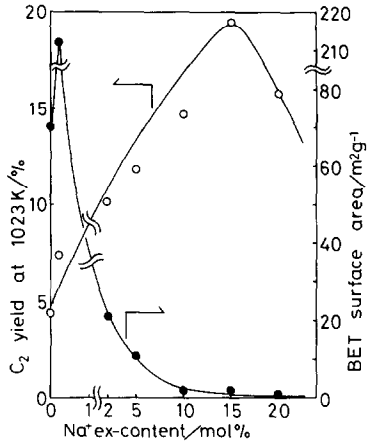

FIG. 1. C_2 hydrocarbon yield at 1023 K and BET surface area as a function of Na^+ expected content in MgO. Methane conversion is 34 to 41%. Percentage of ethene among C_2 hydrocarbons ranges from 50 to 68%.

As alkali compounds are generally volatile, Na^+ and Rb^+ ions are expected to be lost during the heat treatment. Thus, Na^+ and Rb^+ content of every sample was mea-

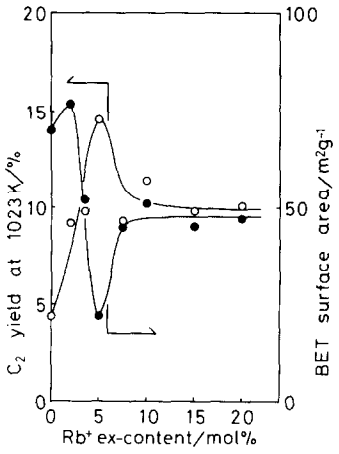

FIG. 2. C_2 hydrocarbon yield at 1023 K and BET surface area as a function of Rb^+ expected content in MgO. Methane conversion is 32 to 38%. Percentage of ethene among C_2 hydrocarbons ranges from 47 to 73%.

sured by AA and ICP before and after a heat treatment–reaction cycle, and the results are shown in Figs. 3 and 4. It is surprising that about 40 ± 10% of Na^+ and 90 ± 10% of Rb^+ are lost during the heating at 1073 K for 3.5 h. It is to be noted that although most of the Rb^+ ion (90%) is lost, an effect of Rb^+ on both specific surface area and C_2 hydrocarbon yield is clearly observed, as shown in Fig. 2. Thus, the structural change effected by alkali doping was examined by other methods such as SEM and XRD.

SEM Observations

Figure 5 shows scanning electron micrographs of the Na^+–MgO catalysts used for the reaction. It is seen that the sample of 0.2% Na^+–MgO is composed of well-developed micropores, which corresponds to the high specific surface area shown in Fig. 1. The samples for which the Na^+ expected content is more than 10% are composed of well-developed crystals. Figure 6 shows scanning electron micrographs of the Rb^+–MgO catalysts used for the reaction. Although these samples have lost most of the Rb^+ ion, morphological changes are observed by SEM. The 5% Rb^+ expected content MgO sample is composed of well-developed crystals (Fig. 6), which correspond to the lowest specific surface area (Fig. 2). The diameters (L) were calculated from the specific surface areas, assuming cubes, or mean particle diameters were obtained for 5 to 10 particles in a micrograph. These values are plotted as a function of Na^+ or Rb^+ expected content in Figs. 7 and 8, respectively. The particle diameters obtained by the two methods agree well for Na^+–MgO samples and agree relatively well for Rb^+–MgO samples (*20*). Thus, the geometrical changes observed by the BET method were verified by SEM. Although the geometrical factor (specific surface area) is clearly important for the effective

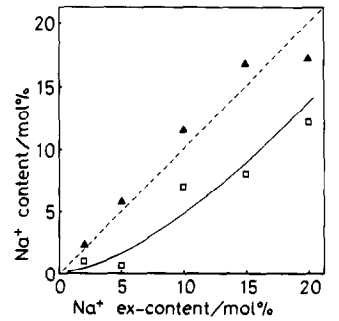

FIG. 3. Na^+ content of Na^+–MgO catalyst after the impregnation (▲) and after the calcination and the reaction (□) as a function of Na^+ expected content. Expected content is defined as the molar ratio Na^+/Mg^{2+} of the starting compounds.

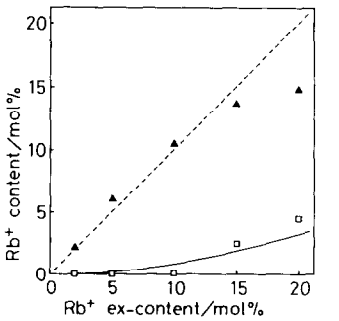

FIG. 4. Rb^+ content of Rb^+–MgO catalyst after the impregnation (▲) and after the calcination and the reaction (□) as a function of Rb^+ expected content. Expected content is defined as the molar ratio Rb^+/Mg^{2+} of the starting compounds.

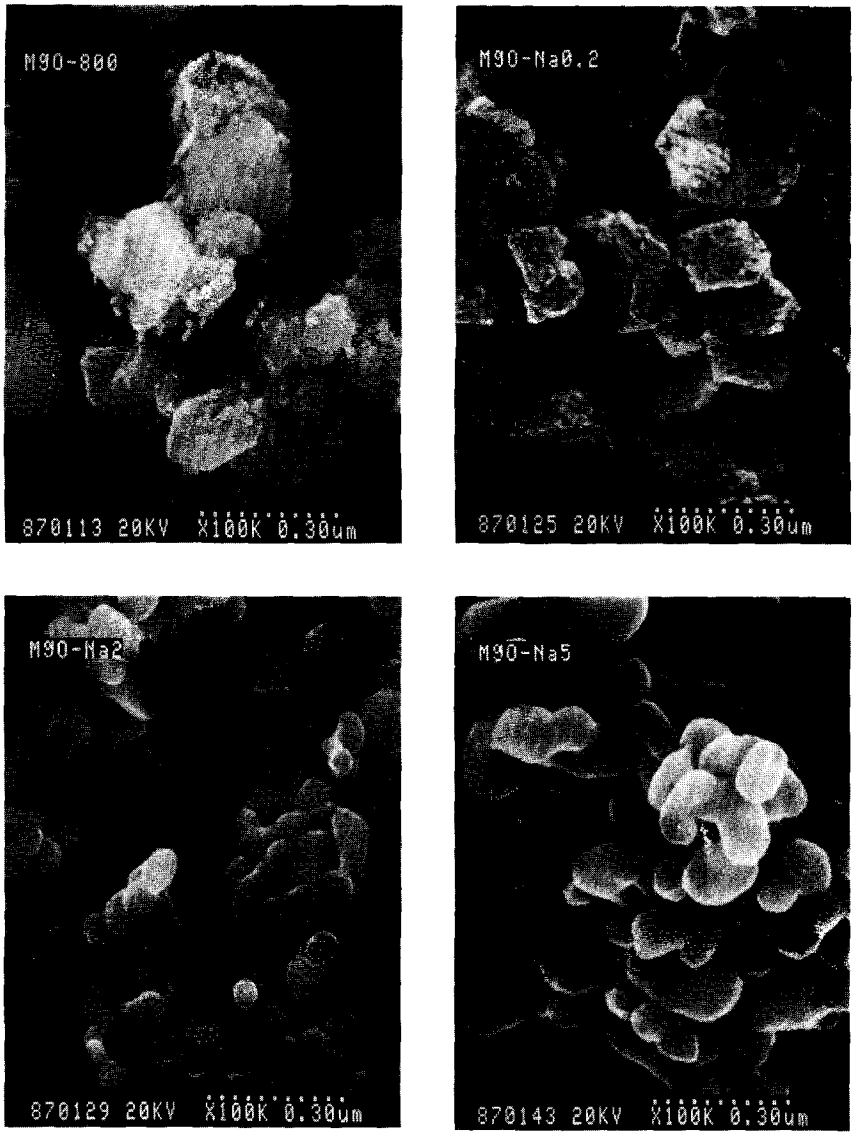

FIG. 5. SEM pictures (clockwise from top left) of MgO, 0.2% Na^+–MgO, 10% Na^+–MgO, 15% Na^+–MgO, 20% Na^+–MgO, 5% Na^+–MgO, 2% Na^+–MgO. One dotted unit corresponds to 30 nm. Na^+ expected content is shown in mol%.

production of C_2 hydrocarbons, there are exceptional cases. When a small amount of alkali is added to MgO, C_2 hydrocarbon yield increases in spite of the fact that the specific surface area also increases as in the case of 0.2% Na^+–MgO (Fig. 1) and 2% Rb^+–MgO (Fig. 2). Thus, the effect of alkali addition was studied by XRD too.

XRD Analysis

Figures 9 and 10 show XRD spectra of the MgO (420) plane for Na^+–MgO and Rb^+–MgO catalysts used for the reaction. The peak width is observed to generally broaden when alkali is added. There is a natural tendency for a sample of greater

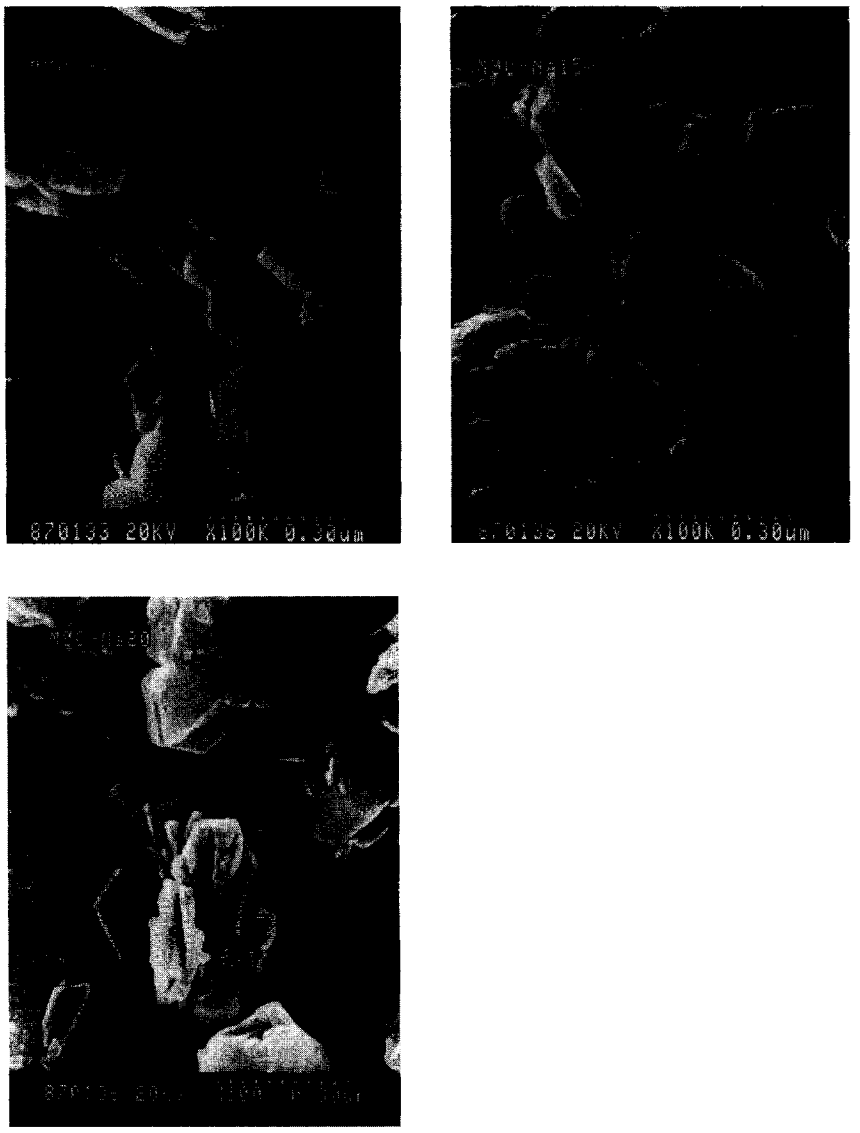

FIG. 5—*Continued.*

particle size to have a narrower peak among *alkali-doped* samples. However, it should be noted that the alkali-doped sample always has broader peaks than the pure MgO. Compare 0.2% or 2% Na^+–MgO with the pure MgO in Fig. 9 and 2% Rb^+–MgO with the pure MgO in Fig. 10 (the last two have almost the same surface area). Thus, for convenience, it is simply assumed that the line broadening is attributable to two factors: *particle diameter* and *lattice distortion*. Generally, line broadening $\Delta(2\theta)$ is related to particle diameter L through Scherrer's equation (*21*)

$$L = \frac{\lambda K}{\Delta(2\theta) \cos \theta_0} \qquad (1)$$

where λ is X-ray wavelength ($\lambda = 0.154$ nm

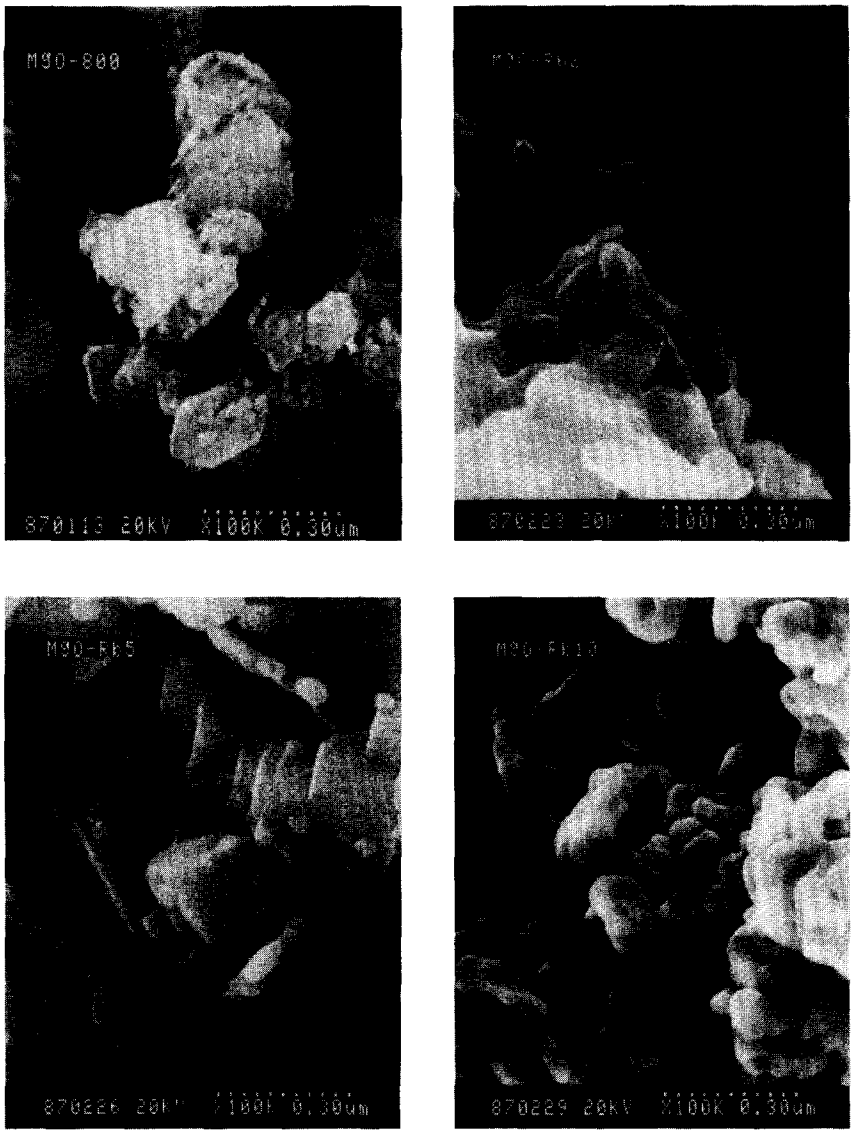

FIG. 6. SEM pictures (clockwise from top left) of MgO, 2% Rb^+–MgO, 15% Rb^+–MgO, 20% Rb^+–MgO, 10% Rb^+–MgO, 5% Rb^+–MgO. One dotted unit corresponds to 30 nm. Rb^+ expected content is shown in mol%.

for Cu$K\alpha$), θ_0 is the diffraction angle ($2\theta_0$ = 109.7°), and K is a constant (0.9). If the *lattice distortion* is supposed to contribute to line broadening, in addition to the *particle diameter,* Warren's equation should be applied (*22*):

$$\Delta(2\theta)^2 = B^2 - b^2. \qquad (2)$$

Here, B is actual line broadening, and b is assumed line broadening which is duc solely to *lattice distortion* and independent of *particle diameter.* In this study, b is assumed to be constant for all samples containing the same kind of alkali promoter. For example, in the Na^+–MgO series, b is assumed to be same as the actual line

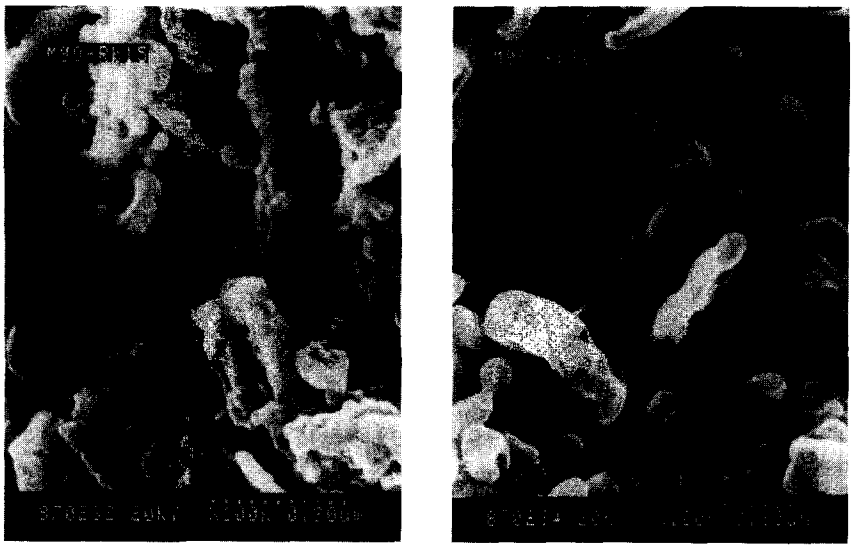

FIG. 6—*Continued.*

broadening (B) of the 15% Na^+–MgO sample (b = 0.0038 rad), because this sample is composed of crystals large enough to conclude that $\Delta(2\theta) = 0$. In the Rb^+–MgO series, $\Delta(2\theta)$ was calculated from Eq. (1) using the particle diameter (BET) for the 15% Rb^+–MgO sample; then b was calculated from Eq. (2) using this $\Delta(2\theta)$ (b = 0.0018 rad). By taking these b values and $\Delta(2\theta)$ which were calculated [Eq. (1)] from particle diameters L(BET), B values were calculated [Eq. (2)] for every sample and are shown (dashed line) as a function of specific surface area in Fig. 11. The observed values of B are also plotted (white and black circles) in the same figure. Both B values are in good agreement for every promoted MgO sample except 0.2% Na^+–MgO. Thus, the above simple assumption seems to be reasonable for the alkali-doped samples of expected contents higher than 2%. Alkali-promoted MgO seems to contain a similar level of distortion independent of the amount of dopant but dependent on the kind of dopant. The pure MgO is considered to have very little distortion or at least less distortion than the promoted MgO, and 0.2% Na^+–MgO is considered to have intermediate lattice distortion. The sample with lattice distortion gives high C_2 yield.

DISCUSSION

Lattice Distortion by Addition of Alkali

For the replacement of Mg^{2+} with an alkali ion M^+ in the MgO crystal, two states, $(M^+M^+O^{2-})$ and (M^+O^-), are supposed in order to neutralize charges in the bulk. Since the alkali ion radius (0.116 nm for Na^+, 0.166 nm for Rb^+) is greater than that of Mg^{2+} (0.086 nm), the above states would cause lattice distortion. However, the difference in radius is so great that very little alkali could be replaced in the MgO crystal. Indeed, 90% of the added Rb^+ ion is lost during calcination at 1073 K. Even for the Na^+ ion, 40% is lost during calcination at 1073 K and some may possibly separate from the MgO phase. However, before calcination, alkali metal ion and Mg^{2+} could be mixed well in the amorphous phase of the hydroxides. During calcination and crystallization of MgO, alkali metal ion may separate. However, at the stage of premature crystallization, alkali metal ion could

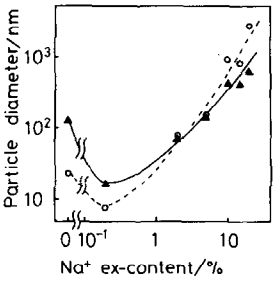

FIG. 7. Particle diameter of Na^+–MgO catalyst measured by both SEM (▲) and BET (○) as a function of Na^+ expected content. Samples are used for the reaction.

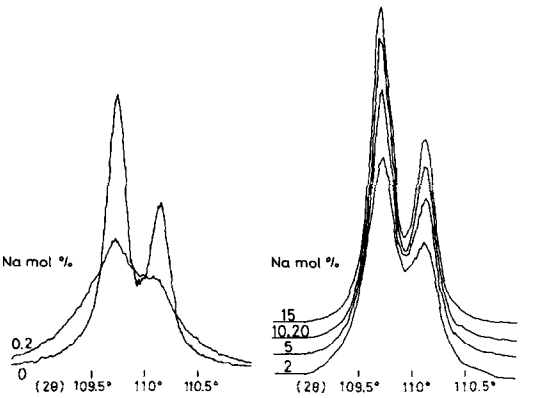

FIG. 9. XRD spectra of Na^+–MgO catalyst used for the reaction.

be present instead of Mg^{2+} ion. Such an intermediate state is considered to affect the final state after the calcination. Indeed, ex(expected)-2 mol% Rb^+–MgO, ex-5 mol% Rb^+–MgO, and ex-10 mol% Rb^+–MgO, which are almost Rb^+ free, show XRD features different from those of pure MgO (Figs. 10 and 11). The MgO sample after interaction with Rb^+ is considered to have a different character, for example, with respect to lattice distortion. The topotactic effect is observed in Figs. 5 and 6, where the MgO crystal, which should be cubic, reflects the precursor hexagonal state of $Mg(OH)_2$ (*23*).

The broader XRD peaks obtained for MgO may not be explained solely by the lattice distortion in the bulk. For example, the surface MgO phase may be modified by interaction with the alkali. The exact model should be the subject of future study.

In addition to the surface area effect, the lattice distortion effect is proposed to explain the reactivity of Na^+–MgO and Rb^+–MgO. Methyl radicals which have been observed over Li^+–MgO (*3c*) or La_2O_3 (*3d*) are considered to be intermediates in this reaction. Some radical initiators would be necessary on the surface in order to produce methyl radicals. Distorted lattices would bear more vacancy or radical centers on the surface. We cannot identify the exact vacancy or radical center; however, it is not considered to be a $[M^+O^-]$ center such

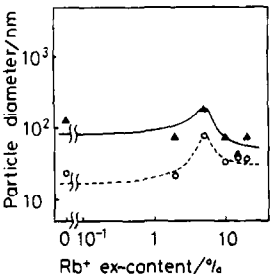

FIG. 8. Particle diameter of Rb^+–MgO catalyst measured by both SEM (▲) and BET (○) as a function of Rb^+ expected content. Samples are used for the reaction.

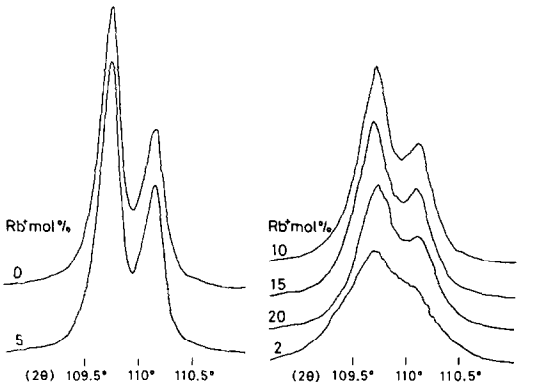

FIG. 10. XRD spectra of Rb^+–MgO catalyst used for the reaction.

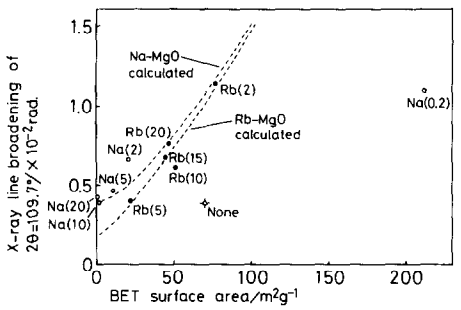

FIG. 11. X-ray line broadening of Na^+–MgO and Rb^+–MgO catalysts as a function of specific surface area. Dashed lines are calculated values based on specific surface area and Eqs. (1) and (2) in the text.

as $[Li^+O^-]$ (*3c*) in this case. Because Rb^+-free MgO samples (2, 5, and 10% Rb^+–MgO), which are more active than pure MgO, they cannot have such centers; further, we failed to observe any $[Na^+O^-)$ center on Na^+–MgO samples after the reaction by a quenching method (*3c, d*). More investigation is required to identify such active centers that give methyl radical from methane. However, we propose that some topotactic result, such as lattice distortion due to alkali addition, produces the radical centers during catalysis. Since the XRD is easily measured, line broadening should be a good measurement to characterize the coupling catalyst.

Specific Surface Area Reduction by Addition of Alkali

The sintering rate of MgO crystals produced by dehydration of $Mg(OH)_2$ has been reported to depend on H_2O vapor pressure and to be related to the amount of lattice defect V_M that accompanies the formation of surface OH^- (*24, 25*):

$$Mg^{2+} + O^{2-} + H_2O \rightarrow Mg^{2+} + 2OH^- + V_M. \quad (3)$$

In this study, line broadening due to alkali addition is ascribed to lattice distortion. As discussed earlier, entrapment of a large amount of alkali ion in the hydroxide state causes lattice distortion during the calcination. Since the distorted lattice contains more defects, Mg^{2+} and O^{2-} ions are considered to be more mobile during the calcination if the lattice is distorted by the alkali doping. The lattice distortion would accelerate the sintering rate.

Relationship between Specific Surface Area and the Reaction

Specific surface area has been pointed out as one of the factors controlling C_2 hydrocarbon production (*5c, d*). It was also found in this study that MgO samples doped with more than 2 mol% alkali have similar levels of distortion but different specific surface areas. C_2 hydrocarbon yield is found to depend on the specific surface area over those promoted MgO samples. Another example is provided by the sample that was sintered intensively (*5c, d*). MgO doped with 0.2% Na^+ and sintered at 1273 K (7 $m^2\ g^{-1}$) yields 9.8% C_2 hydrocarbons (32.8% CH_4 conversion), whereas treatment at 1073 K (212 $m^2\ g^{-1}$) yields 7.4% C_2 hydrocarbons (33.3% CH_4 conversion). Why this reaction depends on the specific surface area is deduced from its nature as a heterogeneous–homogeneous reaction (*5c, 26, 27*).

$$\begin{array}{ccc} CH_4 & \xrightarrow{1} & CO_2 \\ {\scriptstyle 2}\downarrow & {\scriptstyle 3}\nearrow & \uparrow{\scriptstyle 6} \\ 2CH_3 & \xrightarrow[4]{} & (C_2H_6 \xrightarrow[5]{} C_2H_4) \end{array}$$

Heterogeneous: **1**, **2**, **3**, (**5**), **6**
Homogeneous: **4**, **5**

Gas-phase methyl radicals which have been observed over Li^+–MgO (*3c*) and La_2O_3 (*3d*) are considered to be intermediates. Labinger *et al.* have also explained their kinetic results by assuming a gas-phase methyl radical as an intermediate (*14b*). The initial step (path 2) that abstracts hydrogen from methane is considered to occur on active sites, such as surface defects or O^- centers for which the lattice distortion may be a measure. A methyl radical could be oxidized to CO_2 on the surface

(path 3) or undergo recombination in the gas phase to give C_2H_6 (path 4). Path 3 may include an intermediate of CH_3O_2 (*3c*). Since CO_2 is formed over transition metal oxide-doped MgO at lower temperatures without accompanying C_2 hydrocarbons (*5a*), a direct step to CO_2 (path 1) may clearly be the case over less effective catalysts. This path is not important over the catalysts studied in this paper. It is assumed that paths 1, 2, 3, and 6 proceed over a catalyst surface (heterogeneous), whereas paths 4 and 5 proceed in the gas phase (homogeneous). When we compare paths 2, 3, and 4, paths 2 and 3 sould be improved with increasing specific surface area, whereas path 4 should be independent. Thus, a suitable specific surface area would give the maximum C_2 hydrocarbon yield among a series of catalysts depending on the kinetic conditions. A kinetic demonstration of this mechanism is under study. In the MgO system, the suitable surface area would be very small, below 20 $m^2 g^{-1}$. By adding alkali to MgO, the specific surface area is reduced to a suitable value to produce C_2 hydrocarbons effectively. If the above mechanism is applicable, this reaction should be called a heterogeneous—homogeneous reaction (*3c, 5c, 10a*). In this case, surface morphology, which determines the relative ratio of space to surface, should be important.

CONCLUSION

MgO catalysts doped with alkali metal ion were effective for the oxidative coupling of methane even though most of the alkali was lost during the reaction. Alkali addition brings about lattice distortion and specific surface area reduction of MgO. The lattice distortion is considered to increase surface active centers for the production of methyl radicals, whereas the reduction in specific surface area is considered to prevent the deep oxidation of methyl radical to CO_2 and to increase the efficiency of coupling of the methyl radical to C_2H_6 in the gas phase. The characteristic features of these catalysts are well understood if a heterogeneous–homogeneous mechanism is assumed.

ACKNOWLEDGMENTS

We acknowledge Professor T. Onishi, Professor Y. Yamazaki, Professor M. Daimon, and Professor S. Goto for discussions.

REFERENCES

1. Keller, G. E., and Bhasin, M. M., *J. Catal.* **73,** 9 (1982).
2. (*a*) Hinsen, W., and Baerns, M., *Chem. Z.* **107,** 223 (1983); (*b*) Hinsen, W., Bytyn, W., and Baerns, M., *in* "Proceedings, 8th International Congress on Catalysis, Berlin, 1984," Vol. III, p. 581. Dechema, Frankfurt-am Main, 1984; (c) Bytyn, W., and Baerns, M., *Appl. Catal.* **28,** 199 (1986).
3. (*a*) Ito T., and Lunsford, J. H., *Nature (London)* **314,** 721 (1985); (*b*) Ito, T., Wang, J.-X., Lin, C.-H., and Lunsford, J. H., *J. Amer. Chem. Soc.* **107,** 5062 (1985); (*c*) Driscoll, J., Martir, W., Wang, J.-X., and Lunsford, J. H., *J. Amer. Chem. Soc.* **107,** 58 (1985); (*d*) Lin, C.-H., Campbell, K. D., Wang, J.-X., and Lunsford, J. H., *J. Phys. Chem.* **90,** 534 (1986).
4. (*a*) Otsuka, K., Jinno, K., and Morikawa, A., *Chem. Lett.*, 499 (1985); (*b*) Otsuka, K., Liu, Q., Hatano, M., and Morikawa, A., *Chem. Lett.*, 467 (1986); (c) Otsuka, K., Liu, Q., and Morikawa, A., *J. Chem. Soc. Chem. Commun.*, 586 (1986); (*d*) Otsuka, K., Liu, Q., Hatano, M., and Morikawa, A., *Chem. Lett.*, 903 (1986); (*e*) Otsuka, K., and Komatsu, T., *Chem. Lett.*, 483 (1987); (*f*) Otsuka, K., and Komatsu, T., *J. Chem. Soc. Chem. Commun.*, 388 (1987); (*g*) Otsuka, K., Jinno, K., and Morikawa, A., *J. Catal.* **100,** 353 (1986).
5. (*a*) Moriyama, T., Takasaki, N., Iwamatsu, E., and Aika, K., *Chem. Lett.*, 1165 (1986); (*b*) Aika, K., Moriyama, T., Takasaki, N., and Iwamatsu, E., *J. Chem. Soc. Chem. Commun.*, 1210 (1986); (*c*) Iwamatsu, E., Moriyama, T., Takasaki, N., and Aika, K., *J. Chem. Soc. Chem. Commun.*, 19 (1987); (*d*) Iwamatsu, E., Moriyama, T., Takasaki, N., and Aika, K., *in* "Methane Conversion Proceedings, Symposium on Production of Fuels and Chemicals from Natural Gas, Auckland 1987" (D. M. Bibby *et al.*, Eds.), p. 373. Elsevier, Amsterdam, 1988.
6. (*a*) Imai, H., and Tagawa, T., *J. Chem. Soc. Chem. Commun.*, 52 (1986); (*b*) Imai, H., Tagawa, T., and Kamide, N., *J. Catal.* **106,** 394 (1987).
7. (*a*) Matsuura, I., Utsumi, Y., Nakai, M., and Doi, T., *Chem. Lett.*, 1981 (1986); (*b*) Matsuura, I., Doi, T., and Utsumi, Y., *Chem. Lett.*, 1473 (1987).

8. (*a*) Asami, K., Hashimoto, S., Shikada, T., Fujimoto, K., and Tominaga, H., *Chem. Lett.*, 1233 (1986); (*b*) Asami, K., Omata, K., Fujimoto, K., and Tominaga, H., *J. Chem. Soc. Chem. Commun.*, 1287 (1987); (*c*) Fujimoto, K., Hashimoto, S., Asami, K., and Tominaga, H., *Chem. Lett.*, 2157 (1987).
9. Ali Emesh, I. T., and Amenomiya, Y., *J. Phys. Chem.* **90,** 4785 (1986).
10. (*a*) Sinev, M. Y., Vorobeva, G. A., and Korchak, V. N., *Kinet. Katal.* **27,** 1164 (1986); (*b*) Sinev, M. Y., Korchak, V. N., and Krylov, O. V., *in* "Proceedings, 6th International Symposium on Heterogeneous Catalysis, Sofia, 1987" (D. Shopov *et al.*, Eds.), Vol. I, p. 450. *Bulgarian Acad. Sci.*, 1987.
11. Yamagata, N., Tanaka, K., Sakai, S., and Okazaki, S., *Chem. Lett.*, 81 (1987).
12. Imamura, S., Ikehata, M., and Ishida, S., *Chem. Exp.* **2,** 49 (1987).
13. (*a*) Sofranko, J. A., Leonard, J. J., and Jones, C. A., *J. Catal.* **103,** 302 (1987); (*b*) Jones, C. A., Leonard, J. J., and Sofranko, J. A., *J. Catal.* **103,** 311 (1987).
14. (*a*) Labinger, J. A., Ott, K. C., Mehta, S., Rockstad, H. K., and Zoumalan, S., *J. Chem. Soc. Chem. Commun.* 543 (1987); (*b*) Labinger, J. A., and Ott, K. C., *J. Phys. Chem.* **91,** 2682 (1987).
15. Hutchings, G. J., Scurrell, M. S., and Woodhouse, J. R., *J. Chem. Soc. Chem. Commun.*, 1388 (1987).
16. Martin, G.-A., and Mirodatos, C., *J. Chem. Soc. Chem. Commun.*, 1393 (1987).
17. Machida, K., and Enyo, M., *J. Chem. Soc. Chem. Commun.*, 1639 (1987).
18. Roos, J. A., Bakker, A. G., Bosch, H., Van Ommen, J. G., and Ross, J. R. H., *Catal. Today* **1,** 133 (1987).
19. Kimble, J. B., and Kolts, J. H., AIChE Spring Meeting, New Orleans, 1986.
20. Anderson, P. J., and Livey, D. T., *Powder Metall.* **7,** 189 (1961).
21. Scherrer, P., *Gottinger Nachrichen* **2,** 98 (1918).
22. Gallezot, P., *in* "Catalysis, Science and Technology" (J. A. Anderson and M. Boudart, Eds.), Vol. 5, p. 221. Springer-Verlag, Berlin, 1984.
23. Goodman, J. F., *Proc. R. Soc. London Ser. A* **247,** 346 (1958).
24. Eastman, P. F., and Cutler, I. B., *J. Amer. Chem. Soc.* **49,** 526 (1966).
25. Ito, T., Fujita, M., Watanabe, M., and Tokuda, T., *Bull. Chem. Soc. Japan* **54,** 2412 (1981).
26. Shalya, V. V., Kulinich, M. G., and Polyakov, M. V., *Kinet. Katal.* **5,** 916 (1964).
27. Latyshev, V. P., and Popova, N. I., *Kinet. Katal.* **8,** 73 (1967).